

# Effect of self-lubricating carbon materials on the tribological performance of ultra-high molecular weight polyethylene

N. Camacho<sup>a</sup>, J. M. González-Carmona<sup>a</sup>, D. G. Espinosa-Arbeláez<sup>a</sup>, R. Hernández-Bravo<sup>a</sup>,  
J. Muñoz-Saldaña<sup>b</sup>, V. Mujica<sup>c</sup>, and G. C. Mondragón-Rodríguez<sup>a,\*</sup>

<sup>a</sup>CONAHCYT-Centro de Ingeniería y Desarrollo Industrial,  
Av. Pie de la Cuesta, 702, 76125, Santiago de Querétaro, México.

\*e-mail: guillermo.mondragon@cidesi.edu.mx

<sup>b</sup>Centro de Investigación y de Estudios Avanzados del IPN,  
Lib. Norponiente, 2000, Fracc. Real de Juriquilla, 76230, Santiago de Querétaro, Mexico.

<sup>c</sup>Arizona State University, School of Molecular Sciences 551 E,  
University Dr, Tempe, Az, 85281, USA.

Received 31 March 2023; accepted 9 September 2023

For over five decades, ultra-high molecular weight polyethylene (UHMWPE) has been the standard material for total knee replacements (TKR). Zero wear of the UHMWPE would be ideal; however, due to the natural knee movements, wear damage to the UHMWPE articulating surface is inevitable. The generated wear debris results in joint mechanical instability, reduced joint mobility, increased pain, and implant loosening. Because of these issues, the research on the materials in TKRs has increased their survival rate for up to 20 years; however, in younger patients, the durability of the UHMWPE component decreases due to increased physical activity. Hence there is a constant need for highly wear-resistant tribological pairs for TKRs. Carbon-based materials have an excellent balance between lubricating and mechanical properties and have shown great promise in tribological applications. This study used self-lubricating cubic titanium carbide (c-TiC) and multiwalled carbon nanotubes (MWCNTs) to improve the UHMWPE wear resistance further. The combination of carbon-based materials decreased the material loss by about 41.7 % compared to the UHMWPE vs. bare steel ball tribological pair. The improvement, attributed to the c-TiC self-lubricating coating surface, is close to 5 %. Cold flow and burnishing were the predominant wear mechanisms observed in all the systems; more subtle wear processes were detected for the sliding couple with c-TiC self-lubricating coating. Meanwhile, polymer delamination and micrometer-sized debris formation were the main wear mechanisms in the UHMWPE-MWCNT vs. bare steel ball system. The adhesion work obtained from the electronic structure calculations shows a more significant interfacial interaction of the CNTs on the c-TiC surface. This interaction can be associated with the layer formation that protects the surface from wear and friction.

**Keywords:** MWCNT reinforcement; self-lubricating materials; c-TiC; UHMWPE wear; DFT calculations.

DOI: <https://doi.org/10.31349/RevMexFis.70.021002>

## 1. Introduction

According to the World Health Organization, more than 23 million people have rheumatoid arthritis (RA), and experts predict that the number of patients with RA will double by 2030 [1]. Arthritis is the leading condition requiring total joint replacement, the knee being the most affected joint. Total knee replacements (TKRs) restore the joint affected by degenerative diseases. The knee implant consists of a modular design of a femoral component made of a CoCrMo alloy, a tibial plate made of a titanium alloy (Ti6V4Al), and an ultra-high molecular weight polyethylene (UHMWPE) spacer that functions as the articulating surface between the tibial and the femoral components. UHMWPE has also been proposed as a coating tribomaterial for biomedical applications [18]. Due to its mechanical properties and wear resistance, UHMWPE remains the gold standard for articulating surfaces. However, aseptic loosening due to UHMWPE wear debris-related osteolysis is the primary cause of failure in modern TKRs [3–7], limiting the longevity of the implant to 15 - 20 years [8]. In some cases the aseptic loosening may lead to TKR revisions

within 13 to 21 months [9]. As increasingly younger patients need TKRs, rates of osteolysis-induced aseptic loosening are also increasing, along with revision surgeries; this is closely related to the wear resistance of the UHMWPE material.

Ideally, there should be zero wear of UHMWPE in the knee joint; however, the production of wear debris can lead to mechanical instability, reduced patient mobility, increased pain due to the body's biological response to the debris, loosening of the component, and ultimately, failure [10, 11]. In extreme cases where the UHMWPE has completely worn out, the femoral component begins to wear away the tibial baseplate, leading to metallosis (or tibial plate break) [11]. The increasing demand for longer-lasting TKRs, particularly for younger and more active patients, has further motivated scientists and engineers to improve the wear performance of UHMWPE [8].

Different types of nanoparticles have been used to improve the wear resistance and oxidation stability of UHMWPE, these include hydroxyapatite [12], talc particles [13], graphene nanoplates [14], and carbon nanotubes (CNT) [15–18]. There are two types of CNTs: multiwalled (MWC-

NTs) and single-walled carbon nanotubes (SWCNTs). The former consists of two or more concentric cylindrical shells of graphene sheets arranged coaxially around a central hollow core; as in graphite, they exhibit an interlayer separation. In contrast, a single graphene cylinder forms SWCNTs. SWCNTs and MWCNTs have high aspect ratios with diameters close to molecular dimensions and outstanding mechanical properties.

UHMWPE has been blended with small additions of both CNTs to improve the mechanical properties of the polyethylene, such as Young modulus, tensile and yield strength, hardness, toughness, and wear and oxidation resistance [17]. However, SWCNTs concentrations are usually lower, ranging from 0.01 to 0.2 wt. % than those used for MWCNTs (0.1 – 7.5 wt.%). Furthermore, while pristine MWCNTs can significantly improve the mechanical properties of UHMWPE, SWCNTs are usually functionalized. For instance, M. Abdul Samad and S.K. Sinha used air plasma-treated SWCNTs at 0.05, 0.1, and 0.2 wt. % to reinforce UHMWPE coating [18]; as a result, the hardness and elastic modulus increased by 66 % and 58 %, respectively with 0.2 wt. % of SWCNTs. In addition, with increasing SWCNTs concentrations, an increase in scratch and penetration resistance of the polymer was observed. Furthermore, J.M. Diabb Zabala *et al.* [19] studied the effect of 0.01 and 0.1 wt.% functionalized SWCNTs on UHMWPE. The functional group attached to the SWCNTs is not mentioned, however, their results showed an increase of at least 12 % in Young modulus and 65 % in ultimate tensile strength. Moreover, the composite promoted higher osteogenic differentiation than pure UHMWPE.

On the other hand, reinforcement of the UHMWPE with MWCNTs has also been explored as a viable alternative to further improve the polymer performance due to increased mechanical properties [16, 18] and MWCNTs free radical scavenging activity [20, 21]. For instance, A. Fonseca *et al.* [16] used 1 wt. % of pristine MWCNTs by ball milling and obtained a 38 % increase in toughness and an 80 % increase in Young modulus, while Ruan *et al.* [22] enhanced mechanical properties of UHMWPE films by the addition of 1 wt.% MWCNTs, resulting in a  $\sim$  150 % increase in strain energy density,  $\sim$  140 % increase in ductility, and up to 25 % in strength. Following these modifications, significant improvements in wear resistance have also been obtained; however, investigations have been limited to relatively short testing cycles and high (pin-on-disk) normal loads. For instance, Zoo *et al.* tested the UHMWPE-CNT for 2 h at 5 N against a 6.3-mm silicon nitride ball [23], Kanagaraj *et al.* tested UHMWPE-CNT for 16 h at 12 N against alumina balls [24].

Homogeneous distribution of the CNTs in the UHMWPE matrix is crucial to ensure adequate stress transfer between CNTs and the UHMWPE matrix. Single carbon nanotubes coated with polyethylene should produce uniform stress distribution and minimize the stress concentration zones [24]. Recently, it has been demonstrated that 1.25 wt. % MWCNT in the UHMWPE resulted in a decrease in volumetric wear

of 86.9 % after 2 million cycles vs. locally manufactured CoCrMo femoral component under dry conditions [25], suggesting an improvement of the mechanical properties and self-lubricating nature of the composite over the long-term. Other alternatives consider the use of functional coating on UHMWPE [26] and hard solid lubricants such as carbides or carbon-containing such as DLC (diamond-like carbon) on the metallic mechanical counterpart.

The first approaches to developing self-lubricating systems for biomedical applications were suggested long ago. For instance, Teoh *et al.* [27] published evidence that carbon-based systems and surfaces produce friction conditions close to the lubricating graphite vs. graphite surfaces. They developed a composite of titanium and hard titanium carbide (TiC) with varying graphite contents and specific porosity. The concept effectively reduced the coefficient of friction (CoF) (up to 60 %) and the wear on both articulating surfaces. Most of the observed benefits were attributed to the transfer graphite layer and the porosity of the coating. Recently, TiC formed by titanium carburization decreased the CoF and the wear rate UHMWPE in pin-on-plate tribology test [28]. In both cases, the open porosity acted as a system for debris storage. Regarding the application, the TiC coating improved the wear resistance of the femoral head and reduced the wear rate of the UHMWPE cup after 1 million cycles [29]. However, the individual contribution of the TiC coating and the micro-porosity to the wear rate reduction of UHMWPE remains unexplained.

Furthermore, carbon-based and nitride coatings deposited by arc-PVD or magnetron sputtering techniques continue to capture attention as protective coatings to reduce implant friction and wear [30]. However, published results show that the self-lubricating surface was mainly applied to the femoral component or the UHMWPE polymer spacer, and more research needs to be done on using self-lubricating solid materials on both bearing surfaces. For instance, in 2019, S. Deenoi *et al.* reported the tribological performance of a DLC-coated Ti64 alloy surface versus UHMWPE reinforced with 2 wt. % CNTs; they found a higher CoF and significant wear compared to TiN-coated or uncoated Ti64 alloy pins. The behavior was solely attributed to the adhesion of the DLC and the CNTs [31], but no further explanation was given for the wear behavior. Based on the available tribological information of graphite vs. graphite systems, an improvement of the wear resistance based on the carbon vs. carbon self-lubricated interactions could be expected. Therefore, the relationship between self-lubricating carbon-containing UHMWPE composites and hard C-based coated surfaces must be investigated.

The role of Vickers hardness on the wear behavior of UHMWPE for implant applications has been previously reported; this is a crucial aspect affecting the wear rate of the UHMWPE. It has been demonstrated that the wear rate decreases linearly as the surface hardness of CoCrMo bulk and CoCrMo coating materials increases [32]. This decrease in the wear rate is attributed to the resistance of

CoCrMo to being scratched. Therefore, fewer scratches on CoCrMo surfaces could cause fewer scratches and less wear on UHMWPE. Furthermore, the high scratch resistance of alloy systems coated with TiN has also been correlated with lower adhesion to the polyethylene and lower wear of UHMWPE [33] and references therein.

In this work, we investigated the potential of carbon-based self-lubricating materials, such as c-TiC coated on the metal surface and MWCNTs integrated into the UHMWPE to decrease its wear rate further. For this purpose, the wear of UHMWPE-MWCNT nanocomposite against the solid lubricating c-TiC coated counter body was investigated. The research's principal focus was discussing how the c-TiC properties (*i.e.*, average roughness, hardness, thickness, Ti-content, and microstructure) correlate to the wear of UHMWPE-MWCNT. The wear of the UHMWPE composite was analyzed under dry conditions on a reciprocating tribometer of up to 400,000 cycles. Additionally, a first principles computational study was carried out using Density Functional Theory (DFT) to unveil critical aspects of the mechanism of molecular aggregation of the complex system c-TiC, UHMWPE, and carbon nanotubes that can occur during the adhesion process and contribute to the wear of the material.

## 2. Materials and methods

### 2.1. The synthesis of UHMWPE-MWCNT

Multiwall carbon nanotubes (MWCNTs) are commercial products purchased from Skyspring Nanomaterials, USA. The MWCNTs, manufactured by catalytic chemical vapor deposition, displayed an outside diameter ranging from 20 to 30 nm, an inside diameter ranging from 5-10 nm, a length ranging from 10–30  $\mu\text{m}$ , and a purity > 95 %. The polyethylene is a medical-grade UHMWPE GUR  $\text{\textcircled{R}}$ 1020 donated by Ticona Engineering Polymers, Inc. (Bishop, TX, USA). GUR  $\text{\textcircled{R}}$ 1020 displayed a density = 0.930  $\text{g/cc}^3$ , a mean particle size of 137  $\mu\text{m}$ , and an average molecular weight = 3.5 million  $\text{g/mol}$ , according to the manufacturer's specifications.

The preparation of the UHMWPE+MWCNT powder material is described elsewhere [25]. The UHMWPE powder and MWCNTs were mixed by solution blending, allowing MWCNTs agglomerations to disband and form a 3D network inside the matrix. The MWCNTs were then suspended in ethanol and ultra-sonicated for 15 min to break down material clusters. After adding the UHMWPE powder, the mixture was kept in an ultrasonic bath for 45 min. Next, the mixture was mechanically stirred for another 60 min to achieve an even distribution of the MWCNTs. Finally, the mixture was placed in a vacuum oven at 50°C for 24 h to evaporate the alcohol. The distribution of the MWCNTs in the UHMWPE-CNT nanocomposite was observed by scanning electron microscopy (SEM) at 1.5 kV Fig. 1a).

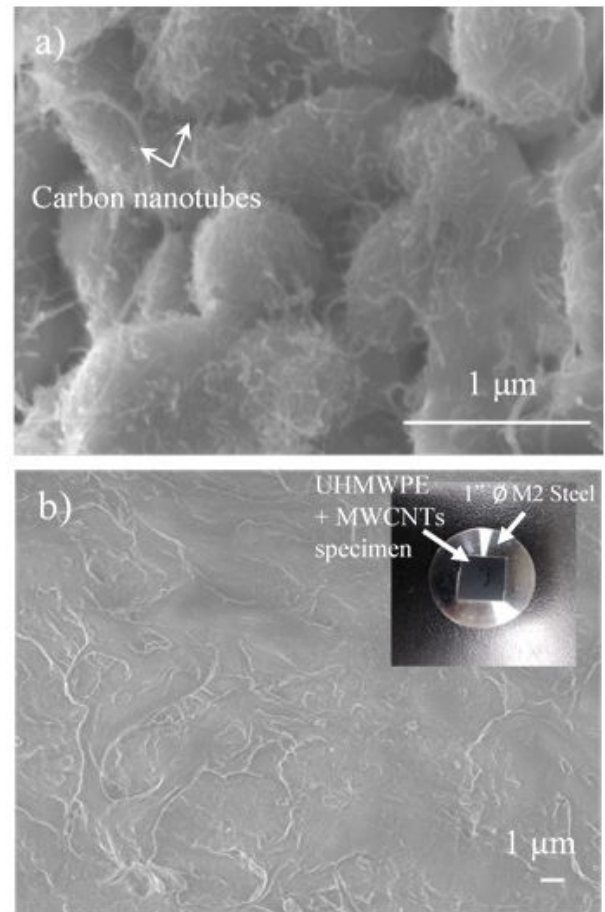


FIGURE 1. a) FE-SEM image of UHMWPE +1.25 wt. % MWCNTs after solution blending. Top-view of the composite UHMWPE +1.25 wt. % MWCNTs fixed in 1 steel coin, inset in and b) FE-SEM image of the initial state of the UHMWPE-MWCNTs surface

### 2.2. Nanocomposite sample preparation

Based on previous results [25, 34], UHMWPE-MWCNT samples were produced with 1.25 wt.% MWCNTs through press molding in a PR-22 Leco mounting press. The powder was pre-compacted at room temperature at a pressure of 24.1 MPa for 20 min in a 38.1 mm diameter mold. The pressure was kept constant throughout the experiment. The press was then heated to 200°C and maintained at that temperature for 15 min. Finally, the press was cooled down to room temperature by air, and the samples were removed from the press and cleaned with ethanol in an ultrasonic bath for 15 min to remove any dust and mold-release lubricant from the surface.

### 2.3. Deposition of the c-TiC coatings

The c-TiC coatings were deposited on mirror polished AISI M2 flat steel samples of 1 inch  $\times$  5 mm high and 6 mm 100 Cr steel precision balls, using an Oerlikon PVD semi-industrial coater, model Domino Mini, and a 99.5 % Ti target (10  $\times$  450 mm) from Plansee. The substrates were ultrasonically cleaned, dried, and mounted on a three-fold rotation

system for proper coating deposition. Once the samples were introduced into the coating chamber, the process started with a 2-h heating-assisted vacuum step to reach  $\approx 450$  °C and  $10^{-5}$  mbar. Then, the sample surfaces were activated with Ar<sup>+</sup> ions at  $10^{-2}$  mbar, applying  $-50$  V DC bias, 20 kHz for 40 min. The substrates were subsequently coated with a  $\approx 0.5$   $\mu\text{m}$  thick Ti layer, hereafter called Ti-interlayer. This coating was magnetron sputtered, applying 7 kW of power with a constant (110 sccm) flow of high purity Ar and 150 V DC bias. Next, a  $\approx 0.2$   $\mu\text{m}$  thin TiN bonding coating was deposited to improve the c-TiC adhesion by applying 7 kW of power with 200 sccm constant flow of high purity nitrogen at 100 V DC bias. Finally, the top layer of  $\approx 0.5$   $\mu\text{m}$  thick c-TiC was deposited by reactive magnetron sputtering of the Ti-target with a mixture of pure acetylene and high purity Ar (80 : 60 sccm). At the same time continuous heating was applied to maintain the chamber temperature at  $\approx 450$ °C using a 9 KW heating system. The substrate temperature was measured using thermocouples located near the planetary. The final step in the coating process was cooling the chamber for 1 h and ventilating it with pure nitrogen.

#### 2.4. Coating microstructural analysis

The c-TiC coating was evaluated using a SmartLab XRD diffractometer from Rigaku in PB/PSA mode Parallel Beam/Parallel Slit Analyzer with grazing incidence angle ( $\omega = 2.5^\circ$ )  $2\theta$  geometry using Cu K $\alpha$  radiation (40 KV, 44 Amp) at a step size of  $0.02^\circ$ . The diffraction patterns were indexed using the X-ray powder diffraction Software PDXL from Rigaku. The microstructure was evaluated in a Field Emission Electron Microscope (FE-SEM) model JSM 7200F from JEOL. Chemical mapping and line scan of the c-TiC coating were acquired in an SEM from HITACHI SU8230.

#### 2.5. Surface evaluation and wear analysis of the tribological pair

##### 2.5.1. Surface preparation and evaluation

The UHMWPE-MWCNT samples were cut into  $10 \times 10$  mm specimens and polished using SiC abrasive paper to decrease the surface roughness produced by the precision cutter and begin the wear tests at similar surface characteristics. The roughness of the UHMWPE-MWCNT samples was measured in a DektakXT Surface Profiler from BRUKER. For this purpose, a stylus type with a  $12.5$   $\mu\text{m}$  radius, 3 mg force, 1.5 mm distance, and  $0.2$   $\mu\text{m}/\text{pt}$  resolution was applied. These measurements were repeated ten times to report the average values of the polished surfaces. The average roughnesses ( $R_a$ ) of a commercially available UHMWPE articulating component manufactured by conventional machining and a mirror-polished CoCr alloy are compared. For profilometer mapping of the c-TiC coating deposited on the precision steel ball, a  $100 \times 100$   $\mu\text{m}$  area was selected (this was the approximate initial contact area between the 6 mm steel ball and the flat polymer surface) with a  $2$   $\mu\text{m}$  spacing between profiles

at 30 sec each with a resolution =  $0.022$   $\mu\text{m}/\text{pt}$ . Fifty traces completed the map applying the hills and valleys strategy in the  $6.5$   $\mu\text{m}$  range. The same profilometer mapping strategy was applied to the bare steel ball.

The hardness Vickers of the steel ball was measured using the Revetest indenter model RST from Anton Paar. For this purpose, the steel ball was fixed inside a bakelite and then analyzed with the indenter. Then, 2 N and 3 N normal loads were applied to guarantee the information. The hardness Vickers calculated by using 3 N was reported here.

##### 2.5.2. Raman spectra of the tribological pair

The Raman spectra of the UHMWPE, UHMWPE-MWCNT, and the c-TiC coating were taken at room temperature in a Raman spectrometer from HORIBA Scientific model LabRAM Evolution, using a 633 nm laser and power of 10 mW. The Raman spectra were recorded after averaging the data within 30 sec acquisition time over the  $500$  to  $3500$   $\text{cm}^{-1}$  spectral range. The peak fitting and Raman position calculations were performed by applying the Pseudo-Voigt peak function.

##### 2.5.3. Nanoindentation tests and topography analysis by scanning force microscopy

The c-TiC coating sample was analyzed by scanning force microscopy to reveal the microstructure at sub-micron and nanometer scales. The coating's hardness and reduced elastic modulus were evaluated in the same area using the nanoindentation method. These measurements were performed on a Hysitron Bruker Triboscope Ti-950 instrument using a 1-micrometer diameter spheroconical diamond tip. The test was carried out using a trapezoidal loading cycle in an open loop mode with a maximum load varying from  $400$   $\mu\text{N}$  to  $10$  mN, maintaining the maximum load for 30 s to evidence stress relaxation phenomena in the coating.

##### 2.5.4. Wear tests of UHMWPE-MWCNT

All specimens were weighed before wear testing. The tribological analysis was performed based on the recommendations of the ASTM F732-17 Standard Test Method for Wear Testing of Polymeric Materials Used in Total Joint Replacements [35]. First, the polished  $10 \times 10$  mm UHMWPE-MWCNT samples were attached to a flat 1-in  $\phi$  steel coin. The wear testing of the so-fixed samples was carried out in a pin-on-disk THT tribometer from Anton Paar. The previously 100Cr Steel precision balls coated with the c-TiC-TiN-Ti multilayer system were used as a counter surface against the flat UHMWPE-MWCNT nanocomposites. The combinations of the tribological pairs involving the UHMWPE-MWCNT composite vs. bare steel surface, or the bare steel ball vs. pure UHMWPE were also tested for comparison. The parameters of the rotary reciprocating wear tests are displayed in Table I. In these sets of experiments, only wear under dry-sliding conditions was considered.

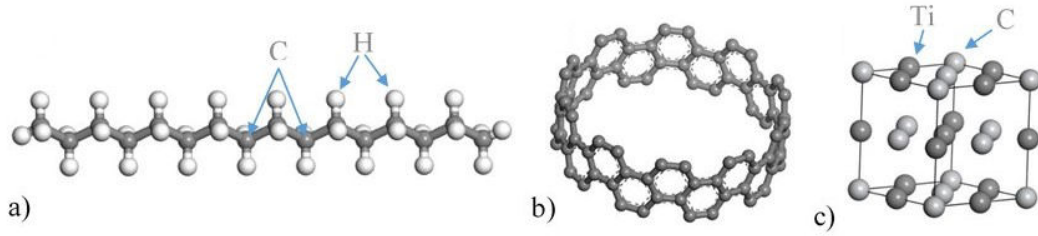


FIGURE 2. a) Structures of the polyethylene chain, b) a single carbon nanotube and c) the cubic FCC structure of the TiC.

TABLE I. Parameter of the wear testing of UHMWPE-MWCNTs vs c-TiC.

Parameter	Value
Radius	1.98 mm
Max linear speed	1.954 cm/s
Frequency	2 Hz
Angle ( $\alpha$ )	90
Load	1 N
Cycles	100, 000, 200, 000 and 400, 000

## 2.6. Theoretical and computational methodology

The electronic structures of c-TiC, polyethylene, and SWCNT were studied within the Density Functional Theory (DFT) framework. A Generalized Gradient Approximation (GGA) with Perdew-Burke-Ernzerhof (PBE) [36] was used within the Cambridge sequential total energy package (CASTEP) code [37]. Electron and core interaction are included using the ultrasoft pseudopotential; atomic positions were optimized until the residual forces achieved a threshold value of 0.01 eV/Å. The integration in the Brillouin zone was performed on special k points ( $8 \times 8 \times 1$  Monkhorst-Pack grid) determined according to the Monkhorst-Pack scheme with a cutoff energy of 350 eV. The model is relaxed by using the BFGS algorithm to optimize the structure. The energy change in the structural optimization process converges to  $2.0 \times 10^{-5}$  eV/atom, and the maximum stress converges to 0.1 eV/Å.

### 2.6.1. Model construction

The c-TiC (111) surface was simulated using the repeated slab geometry with  $(2 \times 1)$  surface unit cell separated by a vacuum region of 20 Å to prevent interactions between periodic images. The model for the cubic phase was obtained from the database in the published literature. These calculated models are shown in Fig. 2. Figure 2a) shows the model corresponding to the polyethylene chain, and Fig. 2b) shows a simplified model of a single-wall carbon nanotube SWCNT. These two elements model the UHMWPE composite. Figure 2c) shows the FCC crystal lattice of the c-TiC that corresponds to the main crystalline structure of the coating. The surface energy ( $\delta$ ) is given by:

$$\delta = \frac{(E_{surf} - nE_{bulk})}{A}, \quad (1)$$

where  $E_{surf}$  is the cell's energy where the surface is contained.  $E_{bulk}$  is the energy of an equivalent number of stoichiometric units of bulk, and A is the surface area. A small positive value of surface energy indicates a stable surface.

The interaction energy ( $E_{int}$ ) for pair of molecules  $i$  and  $j$  was evaluated according to:

$$E_{int} = \Delta E_{int} = E_{ij} - (E_i + E_j), \quad (2)$$

where  $E_{int}$  is the total energy of the interacting systems  $i$  and  $j$ , which can also be seen as the adsorption energy.  $E_i$  is the total energy of the free molecules (corresponding to either the c-TiC surface or polyethylene or SWCNT). Negative  $E_{int}$  values indicate that there exists an effective attraction between them.

### 2.6.2. Adhesive Strength

The adhesion energy ( $W_{adh}$ ) represents the bonding strength of the interface structure and is equivalent to the reversible work required to separate the interface into two free surfaces [38]. The bonding force between the interface atoms increases as the ideal adhesion energy increases. The  $W_{adh}$  is calculated according to the following equation:

$$W_{adh} = -\frac{\Delta E_{int}}{A}, \quad (3)$$

where  $\Delta E_{int}$  is the adsorption energy, and A is the surface area. Similarly, adhesion work is of interest in the area of materials because it can also help predict mechanical properties. For this reason, this computational study intends to determine the adhesion work of the filler components on the c-TiC surface to analyze its effects on the physical properties and wear of the composite.

## 3. Results and discussion

### 3.1. Initial surface quality of the tribological pair

The initial average surface roughnesses ( $R_a$ ) of the mirror-polished UHMWPE ( $\sim 300$  nm) and UHMWPE-MWCNT

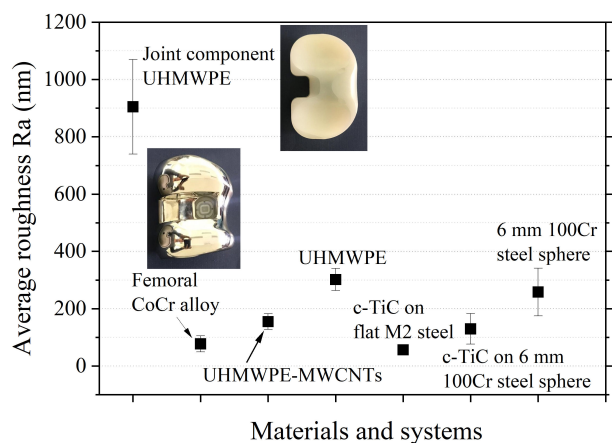


FIGURE 3. Average roughnesses  $R_a$  of UHMWPE, UHMWPE-MWCNTs and c-TiC magnetron coated on flat M2 steel and 6 mm 100Cr steel sphere. These data are compared with commercial and machined UHMWPE joint component and a mirror polished Femoral CoCr alloy.

nanocomposite ( $\sim 150$  nm) are shown in Fig. 3. The presence of MWCNTs improved the surface roughness after polishing under the same conditions as UHMWPE. As a reference, the  $R_a = 900$  nm indicated the level of roughness of a UHMWPE component from a recognized knee prosthesis manufacturer produced by conventional machining. As previously mentioned, the TiC was coated on a flat specimen (used for XRD evaluation) and on a 100Cr steel precision ball, used as the counter body for wear analysis. Figure 3 includes the roughnesses of both samples. The  $R_a$  of the TiC deposited on the previously mirror-polished M2 steel was  $\approx 129$  nm. The initially measured  $R_a$  for the steel ball was

258 nm. The improvement in  $R_a$  indicates that the coating compensated for the imperfections and defects of the commercial precision ball. Figures 4a) and 4a1) show the surface quality of the precision steel ball. The TiC achieved a smooth surface, validated by the high-resolution SEM evaluation. However, Ti-rich splats-like particles were observed on the as-coated surface of the TiC, Fig. 4b). The roughness was measured with force scanning microscopy in the areas where the coating is observed to be homogeneous, revealing values on the order of  $\sim 22.4$  nm, Fig. 4b1). Figure 4b) shows a slightly coarse microstructure of the c-TiC coating on the precision steel balls; these observations correlated well with the  $R_a$  measurements, which were higher for the TiC-coated steel balls than flat steel samples. Further improvements in surface quality can be achieved by optimizing the coating deposition process.

### 3.2. Microstructure and crystalline phases of the c-TiC coating

The tribological response of the UHMWPE-MWCNT is affected by the surface properties of the polymer and the c-TiC-coated counter body. For this reason, the correlation of roughness, the surface microstructure, chemical composition, and the crystallinity of the c-TiC coating is crucial to explain the wear of the UHMWPE-MWCNT composite. Figure 5 shows the most relevant results of the distribution of the chemical elements of the coating. For instance, Fig. 5a) presents the cross-section and thicknesses of the top coating deposited on the Si-wafer. Figure 5b) displays the general distribution of the chemical elements of the coating and the Ti, and C-line scan Fig. 5c) correlates well to the expected

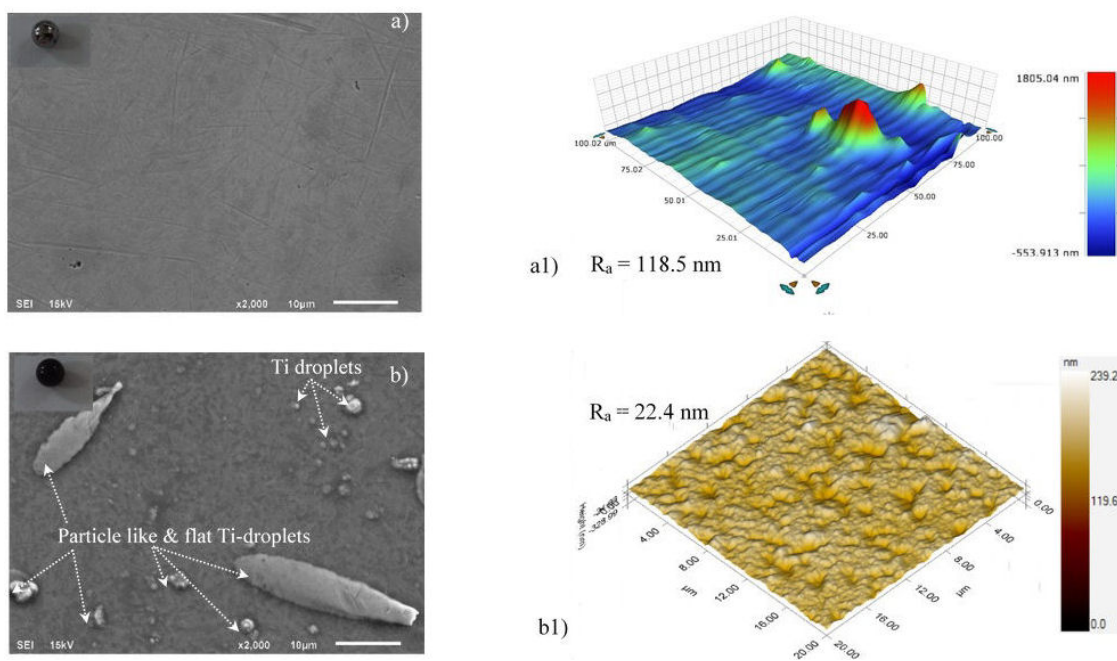


FIGURE 4. a) Surface characteristics of bare precision steel ball and microstructure of the initial c-TiC coating deposited on 6 mm 0 precision steel ball b) and corresponding profilometer or AFM map (right images).

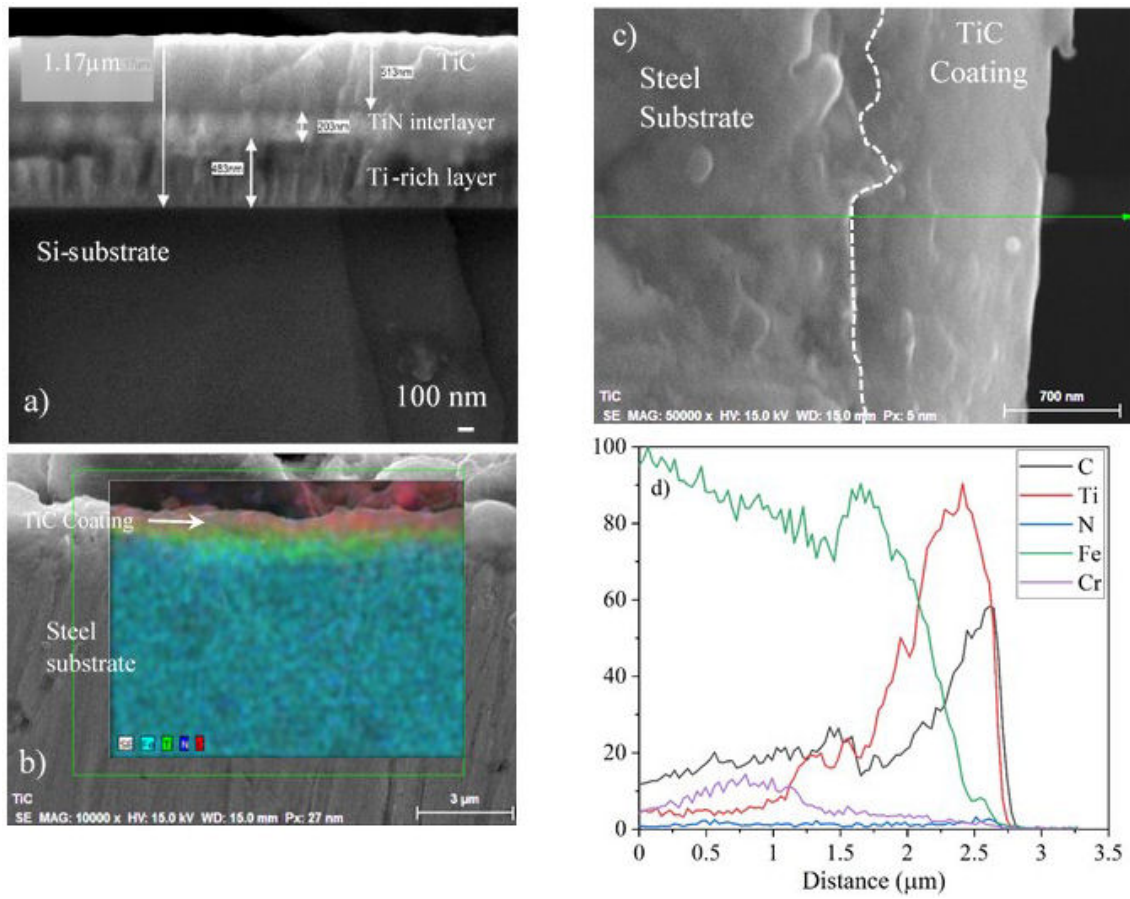


FIGURE 5. a) Cross-section of the c-TiC magnetron sputtered coating on Si-wafer, b) c-TiC on steel ball and c) line-scan.

gradient concentrations Fig. 5d), thus revealing the deposition strategy of the Ti-TiN-TiC system. The Ti-map gradient intensity highlights the C-content in the TiC top layer. This observation agrees with the grazing incidence XRD data shown in Fig. 6. The XRD-graph displays the effect of the incident  $\omega$  angle on the diffraction peaks of the M2 steel-Ti-TiN-TiC substrate-coating system. At high  $\omega$  angles (0.5 - 2.5°), all M2 steel-Ti-TiN-TiC substrate-coating system components contribute to the XRD pattern and are undoubtedly identified. The diffraction patterns present peaks at  $2\theta=36.1$ , 41.88, and 70.32 that correspond to the (111), (220), and (311) planes of the cubic c-TiC in the coating, indicating that this carbide forms due to the reaction between the high Ti-content and the C-species. The XRD measurement also allowed measuring the cubic structure of the TiN interlayer of  $\sim 200$  nm, which is still detected at  $\omega$  angles between 1 and 2.5°. Below  $\omega=1^\circ$ , the TiN was not identified, probably due to the low intensity of the diffraction signal. The diffraction patterns in Fig. 6 also indicate the presence of the metallic Ti-crystalline  $\alpha$  hexagonal phase ( $2\theta=35.02$ , 38.18, 40, 52.64, 62.68, and 75.86). This metallic Ti is mainly related to the Ti-bottom layer. However, metallic Ti microdroplets observed at the outermost TiC layer might also contribute to the diffraction patterns. The  $\omega$  angle was further decreased from 0.5 to 0.1° to extract information only from the c-TiC top coat;

however, this was impossible. The data shows that the XRD beam travels through the coating system and still hits the steel substrate (see diffraction peak M at  $2\theta=44.62^\circ$ ). At such low  $\omega$  angles, the presence of cubic TiC, the TiN, the metallic

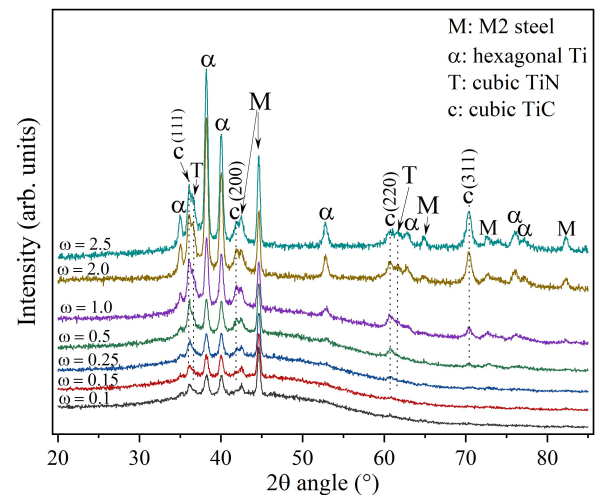


FIGURE 6. The effect of the angle  $\omega$  on the grazing incidence XRD pattern of the TiC top coat/TiN interlayer/Ti bonding coating system.

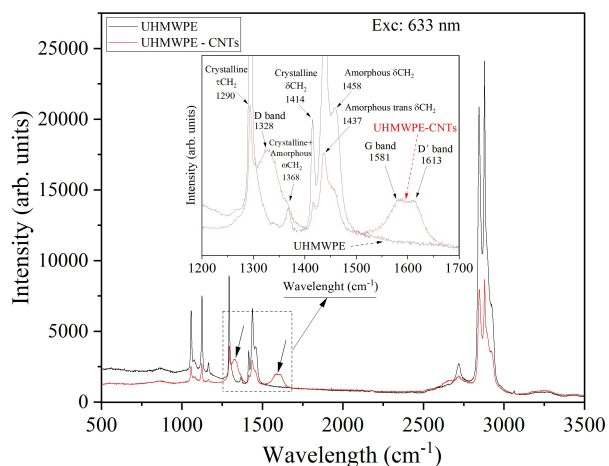


FIGURE 7. Raman spectra of the UHMWPE-MWCNTs.

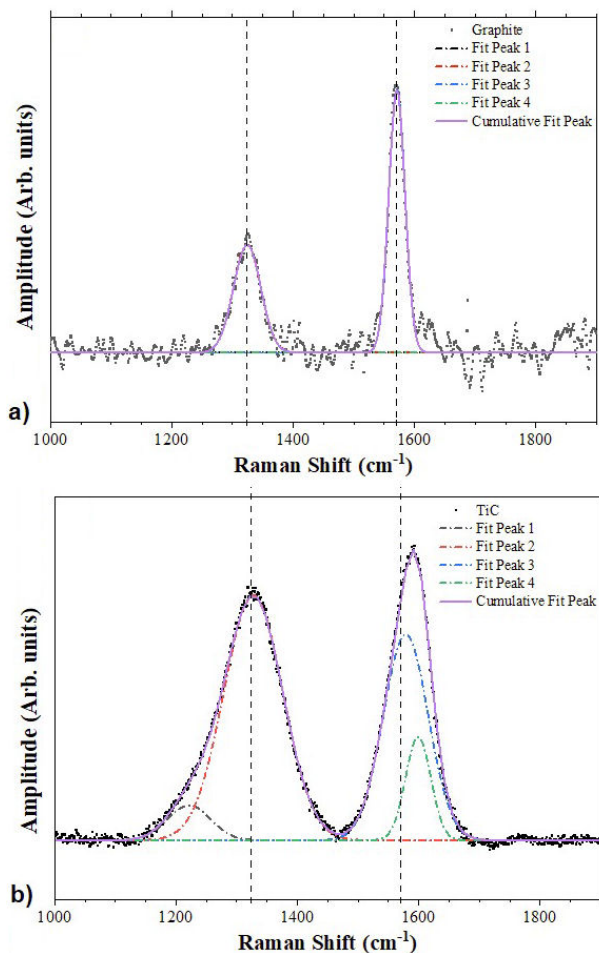


FIGURE 8. a) Raman spectra of graphite, b) compared to magnetron sputtered c-TiC coating.

hexagonal Ti, and the peaks of the steel substrate are still evident. Thus, the diffraction information comes from the bottom Ti-layer ( $\sim 480$  nm) and the TiC top coating ( $\sim 500$  nm). This condition hinders such thin layer's proper selective measurement and phase quantification. Thicker coating are nec-

essary for selective XRD measurement of the outermost top coating.

In carbon-containing coatings, the thickness plays an important role in polymer wear [39]. For example, a  $4.7 \mu\text{m}$  thick carbon-based DLC coating prevented the heat release and increased the UHMWPE wear by  $\sim 60\%$ , while a relatively thin DLC ( $0.8 \mu\text{m}$ ) decreased the wear by  $\sim 41.7\%$ . In addition, the authors reported that the heat produced during friction rapidly dissipates when applying thin coatings. A prosthesis simulator produced these results for a DLC-coated femoral Co28Cr6Mo component after 5 million cycles. On the contrary, in a knee simulator, Oñate *et al.* [40] demonstrated that relatively thick DLCs ( $3 - 4 \mu\text{m}$ ) improve UHMWPE wear; however, they did not mention any heat transfer issues associated with the coating thickness. In the present work, the c-TiC thickness was  $\sim 0.5 \mu\text{m}$ , and no adverse effects on the dry-wear of the UHMWPE or UHMWPE-MWCNT were identified. Using liquid lubricants may also contribute to dissipating the heat caused by friction in the system. However, the optimal coating thickness must be determined after balancing the heat release produced during wear testing and the compressive stresses caused by the film when the coating thickness increases. The increased C-content in the c-TiC layer might also help improve the system lubricity, reducing the probability of any local heating effects.

Published results indicate that the formation of TiC was associated with a substantial transformation of  $\text{sp}^3$  into  $\text{sp}^2$  groups (carbon presence) and high Ti-concentrations (10 to 24.5 at. %) [41]. J. Cui *et al.* [42] investigated Ti + carbon coatings and demonstrated that Ti atoms are present in the metallic form rather than TiC for concentrations of  $\sim 0.41$  at. % Ti. Meanwhile, for concentrations of Ti  $\sim 6.7$  at. %, the formation of TiC is favored, thus producing a composite layer with TiC embedded in the DLC matrix. According to the Ti vs. C phase diagram, the metallic Ti species can only form at high Ti-contents (close to 100 %), and any C-excess will react with Ti to produce the FCC crystalline TiC. For this reason, the carbon source and the chamber designs are additional technical aspects to be considered. For instance, the coatings developed by Cui [42] and ours were deposited by magnetron sputtering in coating chambers close to  $1 \text{ m}^3$  volume, and the significant difference between these processes was the C-source. Moreover, in our process, the analyzed samples were coated while rotating in a 2-axis planetary system, and pure carbide c-TiC and  $\alpha$ -Ti-droplets were identified as the main microstructural features. Q. Wang *et al.* [43] were able to identify the presence of TiC based on characteristic binding energies (BEs) of this compound at relatively low Ti-content  $< 1$  at. %; these low contents are associated with low Ti-target currents during deposition. This coating also displayed the best nano-hardness. In our work, the average point EDX evaluation of the top layer in the c-TiC coating indicated that Ti was  $\sim 5.1$  at. % in the top layer. The calculated Ti-C system phase diagram, using the ThermoCalc methodology, undoubtedly shows that mainly cubic TiC forms in the broad compositional range, for carbon con-

tent < 40 at. %, the stable phase is cubic TiC. The phase diagram also indicates that only hcp-Ti (or  $\alpha$ -Ti) traces are present at temperatures < 500 °C and C-content < 2 mol. %. At the same temperature range and carbon contents > 40 at. %, the single cubic TiC is the thermodynamically stable phase [44]. These observations indicate that cubic titanium carbide forms independently of the C-content and is present in any reactive mixture of Ti+C at processing temperatures below 500°C.

### 3.3. Raman spectra of the self-lubricating surfaces

The self-lubricating capacity of the tribological pair is undoubtedly related to the carbon species contained in the UHMWPE-MWCNT and the crystalline surface of the c-TiC coating. These carbon species might change and evolve upon friction and wear. This section presents and analyzes the chemical state of the carbon species contained in the tribological pair. Figure 7 displays the Raman spectra of the initial state of the UHMWPE and the UHMWPE reinforced with MWCNTs. The intensity loss of the Raman signals is the main spectral feature observed upon adding MWCNTs because the nanotubes are causing the radiation adsorption, decreasing the Raman intensities. However, in both polymer samples, the same Raman signals appear; the band at 1057 and 1124 indicate the C-C stretching; the bands located at 1292, 1368, 1414, 1438, and 1458  $\text{cm}^{-1}$  are related to crystalline  $\tau\text{CH}_2$ , crystalline + amorphous  $\omega\text{CH}_2$  and  $\delta\text{CH}_2$ , amorphous trans  $\delta\text{CH}_2$ , and amorphous  $\delta\text{CH}_2$  species. The observed bands perfectly agree with the reported Raman data of UHMWPE from the literature [45, 46]. The crucial difference is due to the presence of MWCNTs, which produce Raman shifts at  $\sim 1581 \text{ cm}^{-1}$  related to the bond stretching associated with the G-peak (2g mode) of the  $\text{sp}^2$  bonds of carbon rings (aromatic C-species) and chains. The D-peak at  $\sim 1328 \text{ cm}^{-1}$  is due to the breathing mode (A1g mode) of the  $\text{sp}^2$  bonds of only carbon rings. An additional Raman shift is observed at  $1613 \text{ cm}^{-1}$ , which is related to intercalated graphite compounds and is assigned to in-plane vibrations of the other parts of graphite domains. This D' band does not exist in pure graphite [47]. These Raman bands related to the G, D, and D' carbon species of the MWCNTs are not present in pure UHMWPE. Similarly, the c-TiC coating displays two well-defined Raman signals. These bands are due to the D-peak observed at  $1321 \text{ cm}^{-1}$  and the G-peak found at  $1591 \text{ cm}^{-1}$ , Fig. 8. The observed Raman shifts correspond to those features found in magnetron sputtered a-C [48].

### 3.4. Mechanical properties of c-TiC coating

Figure 9 shows typical nanoindentation results through a load versus displacement curve of the coating at maximum penetration depth conditions on the order of 60 nm. The maximum hardness and reduced elastic modulus obtained are 7 and 66 GPa, respectively. These values are lower than those reported in the literature for c-TiC coatings [49,50]. How-

ever, more recently, a decrease in hardness have been reported upon the presence of Ti-contents > 70 at. % [51]. The authors reported 9 ~ 10 GPa for TiC containing 90 to 95 at. % Ti. Additional reasons may be the following. The microstructural characteristics of the c-TiC coating, and according to the thickness measurements shown in Fig. 5a) the c-TiC coating is  $\sim 400 \text{ nm}$  with columnar features and grain

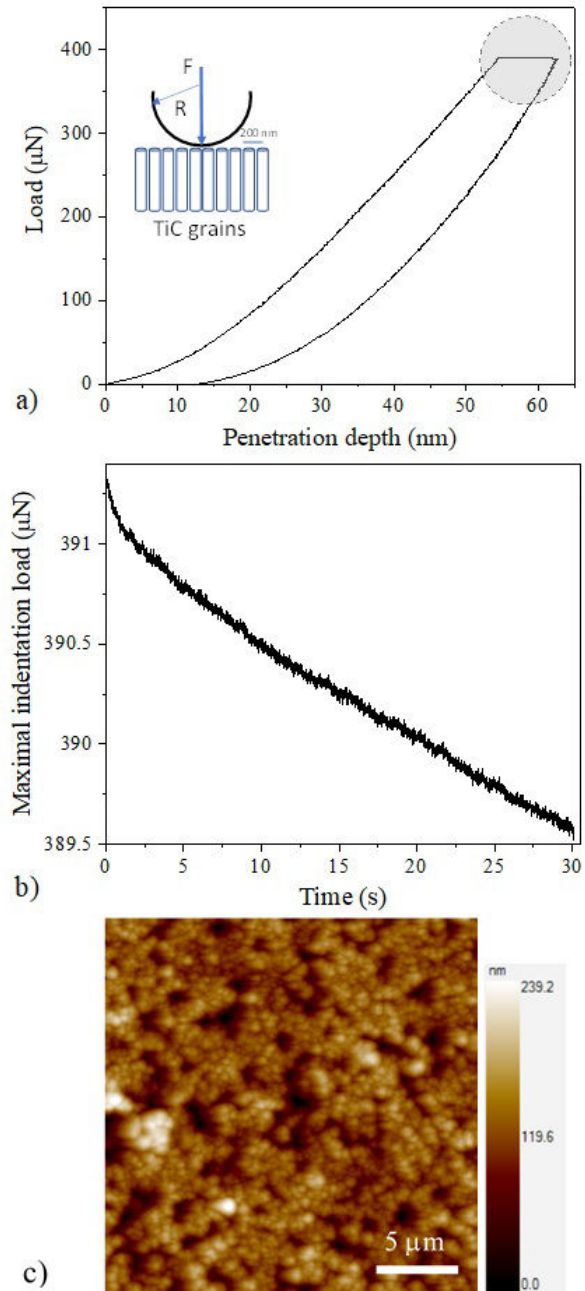


FIGURE 9. Mechanical properties of the c-TiC coating systems measured by nanoindentation, load-penetration curve with a  $P_{max}=400 \text{ mN}$ . a) A schematic representation of the indenter tip radius is shown in the inset. b) Relaxation phenomena (reduction in load as a function of time) and c) SPM micrograph of the surface.

diameters of  $\sim 100$  nm. Under these microstructural arrangements, the c-TiC coating presents a load relaxation phenomenon upon nanoindentation. This phenomenon is schematized in the inset of Fig. 9a) by comparing the dimensions of the radius of the indenter and the columnar c-TiC grains in the coating. Figure 9c) shows a surface micrograph obtained by force scanning microscopy of the coating surface. These micrographs reveal a conformal microstructure with nanometer grains of an average size of 50 nm with pores of similar sizes of equiaxial morphology in the plane but showing columnar features in the depth. The load relaxation phenomenon consists of a reduction of the maximal indentation load as a function of time, Fig. 9b). In the time interval tested, a steady state was not reached at the maximum force, which is expected not to change as a function of time for continuous solids. This relaxation phenomenon is associated with the compliance in the coating plane that occurs under the application of loads, which causes a displacement of the grains laterally and is a function of the applied force and the contact time. This phenomenon, apart from causing an apparent decrease the mechanical properties of the coating, can diminish the friction coefficient, in this case between the indenter and the coating, which can be interpreted as a self-lubrication.

### 3.5. Wear of the UHMWPE-MWCNT vs. c-TiCs

The present work aims to investigate the UHMWPE-MWCNT nanocomposite potential as a self-lubricating material against c-TiC-coated solid lubricant surfaces. In this sense, rotary reciprocating tests were initially designed to provide information about the early stages of UHMWPE wear. The first target was to reach 100,000 cycles and evaluate the corresponding wear modes of UHMWPE vs. c-TiC coated materials. Fig. 10 displays the CoF obtained under a reciprocating movement during 100,000 cycles of the UHMWPE polymer against a 6 mm bare steel ball and the c-TiC coated ball. The CoF of the tribological pair, UHMWPE vs. bare steel ball, starts at about 0.05 and then increases quickly to  $\sim 0.075$ , see Fig. 10a). After this point, there is a steady increase for over 50,000 cycles where the CoF is maintained close to 0.1 in one reciprocating direction (the blue dotted lines in Fig. 10a) and 10b) represent this point) and increased slightly above the  $\text{CoF} = 0.1$  up until 100,000 cycles. After that, the CoF level reaches  $\sim 0.125$  on the opposite side and only increases smoothly up to 100,000 cycles. Considering the applied normal load of 1 N, these CoF imply tangential forces ranging between 0.1 and 0.125 N. Figure 10b) depicts the CoF of UHMWPE vs. c-TiC coated steel ball. In one reciprocating direction, the CoF was close to 0.1, while in the opposite direction, the CoF was markedly below 0.1. Initially, the CoF decreased continuously within the  $\sim 5,000$  cycles, then increased to 10,000 cycles, and after this wide maximum, the CoF fell again before reaching 30,000 cycles. After that, the CoF remained steady at  $\sim 0.0725$ . In this tribological pair, the tangential forces are

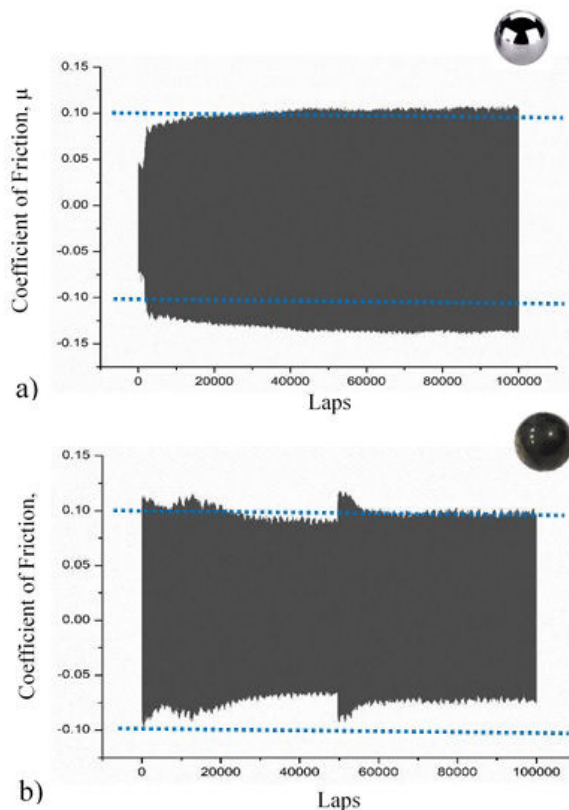


FIGURE 10. a) Coefficient of friction during 100,000 cycles of UHMWPE vs bare steel ball and b) UHMWPE vs c-TiC coated steel sphere. Reciprocant movement, 90, 2 Hz, and 1 N normal load.

$\sim 0.0725$  N. At this point, there is 27.5 % less tangential force when applying the c-TiC coating. Finally, at  $\sim 50,000$  cycles, a CoF peak, almost at 0.1, appeared in one direction and exceeded the 0.1 level in the opposite reciprocating direction. Considering this maximum CoF produced with the TiC, there is a 20 % less tangential force than the tribological pair without the self-lubricating coating. The wear-track evaluation after 100,000 cycles indicated neglectable wear since no mass loss was registered. Additionally, the contact profilometry of the wear tracks demonstrated that scratches were, on average, within the initial surface roughness.

No mass-loss and wear volumes were recorded on the polyethylene without reinforcement UHMWPE and the UHMWPE-MWCNT nanocomposite after 200,000 cycles. This condition changed after 400,000 wear cycles. Figure 11 shows the wear tracks produced on the UHMWPE-MWCNT nanocomposite against the c-TiC-coated steel ball counter body vs. the bare steel ball. These images display a smooth wear track by a c-TiC-coated steel ball [Fig. 11a)] vs the deeper scratches on the wear tracks caused by uncoated steel [Fig. 11b)], agreeing with the mass loss registered in Table II. There was a wear resistance improvement with MWCNTs reinforcement, reflected by the mass loss decrease of  $\sim 36.8$  %. A  $\sim 41.7$  % mass loss decrease was recorded for UHMWPE-MWCNT nanocomposite against the self-lubricating c-TiC

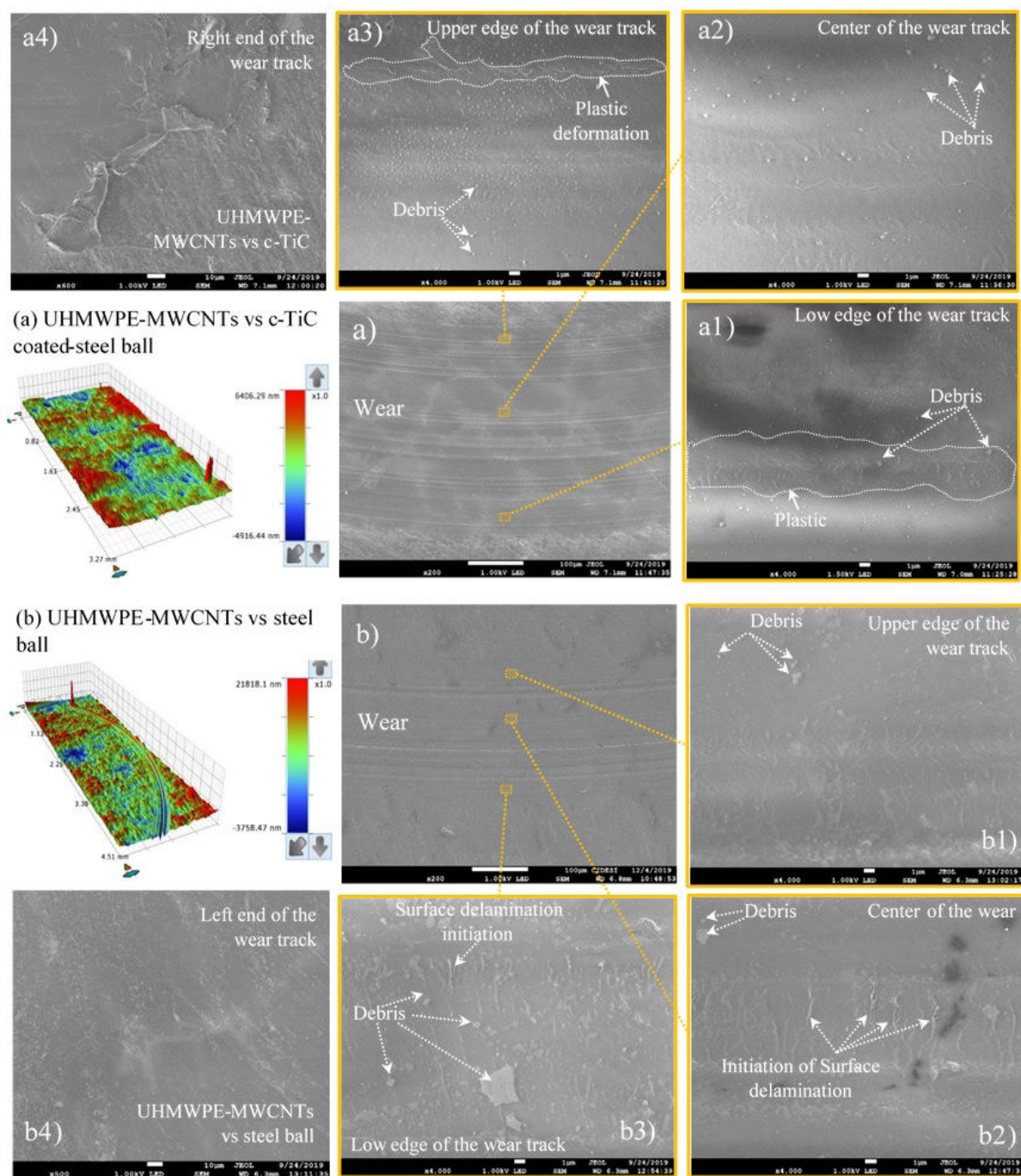


FIGURE 11. a) Profilometry and FE-SEM images of the wear-track of b) the UHMWPE-MWCNTs vs c-TiC coated precision steel ball compared with reference system UHMWPE-MWCNTs vs bare steel ball

coating as the counterface. These results correlate well with the CoF of the analyzed systems. The lowest CoF ( $\sim 0.2$ ) was measured when applying MWCNTs and c-TiC as self-lubricating materials, resulting in the lowest material loss of the UHMWPE-MWCNT composite.

In contrast, the UHMWPE-MWCNT nanocomposite against bare steel produced a CoF  $\sim 0.24$ . The improvement in wear resistance is also evident in the wear-track evaluation made by contact profilometry shown in Figs. 11a) and 11b), showing less wear damage in the UHMWPE-MWCNT vs. c-

TiC system than in the UHMWPE-MWCNT vs. steel pair; this is attributed to the self-lubrication capacity of the MWCNTs and which has been reported as an effective lubricant additive [49]. As mentioned earlier, the use of TiC has been reported to decrease UHMWPE wear damage [50]. The presence of c-TiC, produced after carburization of the Ti femoral head, decreased UHMWPE wear of a joint cup. The debris produced in the UHMWPE-MWCNT and c-TiC nanocomposites and their carbon species must be further investigated. Furthermore, the tribological and chemical effects of liquid

TABLE II. Weight loss and volume loss after wear testing of UHMWPE-MWCNTs vs c-TiC system after 400,000 cycles. Reciprocant movement at 90 and 1 N normal load under dry conditions.

Tribological pair	Mechanical properties	Weight-loss (mg)	Wear improvements based on weight-loss
UHMWPE vs bare steel ball	UHMWPE 64.6± 0.71 in shore D scale Steel ball 998.5 HV <sub>0.3</sub>	1.9	System without self-lubricating components
UHMWPE vs bare steel ball	UHMWPE 63.9± 0.33 in shore D scale	1.2	36.8 %-compared to UHMWPE vs bare steel ball
UHMWPE-MWCNTs vs c-TiC coated steel	UHMWPE-MWCNTs, 63.9± 0.33 in shore D scale c-TiC/TiN/Ti coating system hardness = 7 GPa and $\epsilon = 66$ GPa	0.7	41.7%-compared to UHMWPE-MWCNT vs bare steel ball 65.16%-compared to UHMWPE vs bare steel ball

TABLE III. TiC based coatings for wear reduction of UHMWPE. Coatings characteristics and tribological testing conditions for orthopedic implant applications (hip and knee prosthesis).

Tribological System	Tribological conditions	Improvements
c-TiC/titanium alloy	Pin on Plate, 4 mm pin diameter, 9.8 N normal load, 14.4 m Lubricant 25% Bovine serum and dry	CoF: 0.07-0.085e Dry: 44.5% wear decrease Bovine serum: 66.8%
c-TiC/Ti6Al4V	Artificial joint hip simulator, peak 784 N, 1 Hz Lubricant 25% Bovine Serum + 0.1% sodium azide	Decrease the wear UHMWPE joint cup, TiC could effectively control the UHMWPE debris distribution
c-TiC/TiN/Ti on 6 nm Cr-stell ball vs UHMWPE	Pin on Disk, reciprocating movement, 2 Hz 90, 1 N, 100,000 and 200,000 cycles	CoF ~ 0.1 ~ 0.125 No mass and volume loss registered in both cases
c-TiC/TiN/Ti on 6 nm Cr-stell ball vs MWCNTs-UHMWPE	Pin on Disk, reciprocating movement 2 Hz 90, 1 N, 400,000 cycles 1584 m	CoF ~ 0.2 UHMWPE vs stell $6.0561 \times 10^7$ nm <sup>3</sup> /Nm MWCNT-UHMWPE vs stell $3.9348 \times 10^7$ nm <sup>3</sup> /N MWCNT-UHMWPE vs c-TiC $3.41128 \times 10^7$ nm <sup>3</sup> /N

lubricants simulating articulating joints' wear conditions should also be addressed.

The details of the wear tracks produced after 400,000 cycles on the UHMWPE nanocomposite are in the FE-SEM micrographs, Figs. 11a) and 11b). In the UHMWPE-MWCNT vs. c-TiC tribological pair, there is burnishing of the surface and local plastic deformation (Fig. 11a1)) in the center and along the edges of the wear track. In this system,

only nanometer-sized debris was observed Figs. 11a2) and 11a3). The plastic deformation of the UHMWPE-MWCNT is observed at the end of the wear track of the UHMWPE-MWCNT vs. c-TiC, Fig. 11a4). Less debris and no particle detachment after 400,000 cycles indicate the improvement of UHMWPE wear resistance. In contrast, the UHMWPE-MWCNT displays significant wear surface damage caused by the bare steel, Fig. 11b). There were no apparent signs of

plastic deformation in this tribological system; however, major scratches and higher amounts of micrometer-sized debris due to the progressed surface delamination were observed, Figs. 11b1) to 11b3). High doses of UHMWPE debris in a size range between 0.3 and 2 micrometers, have been reported as critical for biological response (bone resorbing), [8, 52]. The surface delamination initiation was markedly found at the center and the lower edge of the wear track produced on the UHMWPE-MWCNT, Figs. 11b2) and 11b3). The evaluation of the end of the wear track also indicated that no plastic deformation instead of took place, Fig. 11b4).

Table III summarizes primary TiC coating characteristics and the obtained tribological results against UHMWPE in published literature; this information is compared to our results. An objective analysis of the reported UHMWPE wear caused by surfaces made out of TiC is complicated due to the variety of TiC characteristics (thickness, roughness, chemistry) and the selected tribological conditions (the type of testing, normal pressure, number of cycles, environment) or intended application (*i.e.*, hip or knee implants). Therefore, basic linear reciprocating wear motion analysis of CoF and polymer wear rates of potential materials should be carried out according to the norm ASTM F732 (Annex A1.1) [35]. Following the guidelines and recommendations within this standard shall allow proper evaluation and comparisons of CoFs and polymer wear rates. In addition, further rotary reciprocating tests of the UHMWPE-MWCNT vs. c-TiCs at higher wear cycles (minimum half a million, 1 million, and 2 million) + lubricant should be performed to evaluate the response of the material, particularly the corrosion resistance of the coating. This study detected no transfer layer or surface damage on the c-TiC coating.

### 3.6. The work of adhesion calculations

The physicochemical interaction of atoms and molecules of the tribological pair defines friction and wear processes at the nanoscale. For this reason, in the present investigation, the interaction between the surfaces of single crystalline structures of the tribological pairs (UHMWPE, CNT, and c-TiC) is simulated via the first principle of Density Functional Theory (DFT) to evaluate their chemical affinity and work of adhesion between the self-lubricating surfaces at the nanoscale.

#### Energy of TiC(111) slab

The need to study c-TiC is mainly based on the fact that it has excellent mechanical properties and contains C, which is a natural solid lubricant. These characteristics of c-TiC will contribute to the work of adhesion at an atomistic level. They will provide insight into the wear behavior of the polyethylene with and without carbon nanotubes. The c-TiC (111) surface was built in our calculations based on Ti terminations at the system's border, since these are the most thermodynamically stable. This crystalline c-TiC (111) planes' surface energy was calculated to validate the system with reported

TABLE IV. Work of adhesion  $W_{adh}$  (J/m<sup>2</sup>) of the tribological pair

Surface	Polyethylene	SWCNT
$W_{adh}$ (J/m <sup>2</sup> )	3.464	5.379

values in the literature. The results show that the surface energy of the c-TiC (111) plane has a value of 2.606 J/m<sup>2</sup>, which is within the range of reported values [1.35 – 3.13] J/m<sup>2</sup> for the surface energy of the c-TiC (111) plane with Ti terminations [53], proving the reliability of our calculations that validate our computational methodology.

### The work of adhesion of the tribological pair

The work of adhesion ( $W_{adh}$ ) of the tribological pairs investigated here is shown in Table IV. The  $W_{adh}$  between the c-TiC (111) plane and the polyethylene displays a lower  $W_{adh}$  compared to the work of adhesion between the c-TiC (111) plane and the simplified carbon nanotube (SWCNT). Figure 12 shows the schematics of the simplified system consisting of the c-TiC (111) plane vs. the UHMWPE [Fig. 12a)] or the CNT 12b) applied for  $W_{adh}$  calculation, this indicates a weaker interaction between the c-TiC (111) plane and the polyethylene, pointing out the lower affinity and less capacity to build a lubricant protective transfer layer. In contrast, there is a stronger affinity between the c-TiC(111) plane and the surface of the CNT due to the molecular interaction between the Ti and C atoms and the forces coming from the  $\pi - \pi$  bonds of the carbon nanotube; this also shows a high electron transfer between the c-TiC (111) and the carbon nanotube. The strong electronic affinity and the resulting higher interfacial energy or  $W_{adh}$  might cause a protective transfer carbon-based layer formation on the c-TiC (111) plane that induces the self-lubrication effect, contributing to the better wear-performance of the C-containing surfaces.

## 4. Conclusions

- The magnetron sputtering reactive semi-industrial process was applied to deposit the self-lubricating c-TiC. This c-TiC coating was deposited at 450°C produced a reasonably smooth surface (129 nm) that compensated the roughness (258 nm) of commercial precision steel balls applied for rotary reciprocating pin-on-disk wear tests of UHMWPE.
- The outermost surface of the carbon-containing coating comprises cubic TiC and traces of metallic Ti-droplets made of the hexagonal  $\alpha$  Titanium phase.
- The Raman spectroscopy indicates the presence of bands due to the G, D, and D' carbon species of the MWCNTs contained in the UHMWPE-MWCNT composite. In contrast typical amorphous carbon a-C species are obtained in the sputtered coating.

- The c-TiC coating is based on a conformal-like microstructure with grains showing columnar features of  $\sim 50$  nm with pores of similar sizes of equiaxial morphology in the plane. This microstructure allows a load relaxation phenomenon consisting of a reduction at the maximal indentation loads as a function of time. This phenomenon is also contributing to self-lubrication during wear.
- Neglectable effects on the wear track were observed after 100,000 and 200,000 reciprocating wear cycles.
- As expected, the addition of 1.25 wt.% MWCNTs improved the UHMWPE wear resistance by  $\sim 36.8$  % after 400,000 cycles of rotary reciprocating sliding under dry conditions and 1 N normal pin-on-disk load against bare stainless steel. The homogeneous distribution of the MWCNTs creates a 3D network around the UHMWPE powder; this mechanical bonding between both materials might be responsible for wear resistance improvement.
- The UHMWPE-MWCNT mass loss was improved by  $\sim 41.7$ % when applying the lubricating c-TiC coated steel compared to the reference system (UHMWPE vs. Steel). This result represent 4.9 % less wear than the system without coating and is mainly attributed to the lubricating coating surface finish of c-TiC.
- A smooth wear-track and relatively low CoF  $\sim 0.2$  were obtained in the UHMWPE-MWCNT vs. c-TiC coated ball, deeper scratches and slightly higher CoF  $\sim 0.24$  in the UHMWPE-MWCNT vs. bare steel ball were obtained.
- Submicrometer-sized debris and mild plastic deformation were observed in the UHMWPE-MWCNT vs. c-TiC coated steel ball. In contrast, submicrometer and micrometer-sized debris, critical for the biological response, and signs of surface delamination in the wear

track produced in the UHMWPE-MWCNT vs. bare steel ball.

- The theoretical calculations indicated that the  $W_{adh}$  between the (111) plane surface of the c-TiC and the carbon nanotube is higher than the  $W_{adh}$  between the c-TiC and the polyethylene, thus indicating the formation of a transfer carbon layer on the (111) plane of the c-TiC coating that might contribute to a better wear performance.

## Acknowledgments

Financial resources and materials were partially provided through the FORDECYT projects 297265 and 296384 and the project 2015 – 02 – 1077 Frontiers of Science program managed by CONAHCYT.

The authors kindly thank the National Laboratory CENAPROT-(sede CIDESI) for providing all the facilities and access to the PVD unit for c-TiC development, and the characterization instruments. The authors also thank Ticonacel Celanese Corporation for providing the UHMWPE for this research.

N. Camacho, J.M. González-Carmona, R. Hernández-Bravo, and G.C. Mondragón-Rodríguez acknowledge the support from CONAHCYT through their research Fellowship Investigadores por México before C tedra CONAHCYT.

The authors acknowledge Dr. J.M. Alvarado-Orozco for proofreading the first version of the manuscript.

Thanks to C. Ortega, M. F. Lara P rez, and J. D. Escobedo Rodr guez for their support the tribological tests and Armando Dom nguez for c-TiC coating preparation.

The authors acknowledge the support and access to the micro-Raman instrument at Cinvestav Quer taro facilitated by Ing. F. Rodr guez Melgarejo and Dr. S. Jim nez Sandoval.

The authors appreciate the access and support provided by Ing. Manuel Aguilar and Dr. Rodrigo A. Esparza from the Laboratorio Nacional de Caracterizaci n de Materiales (LaNCaM)- UNAM Quer taro.

- 
1. Global RA Network About Arthritis and RA <https://globalranetwork.org/>
  2. M. Abdul Samad, Recent Advances in UHMWPE/UHMWPE Nanocomposite/UHMWPE Hybrid Nanocomposite Polymer Coatings for Tribological Applications: *A Comprehensive Polymers*, **13** (2021) 608.
  3. E. M. Brach del Prever, A. Bistolfi, P. Bracco, and L. Costa for arthroplasty: past or future?, *Journal of Orthopaedics and Traumatology*, **10** (2009) 1. <https://doi.org/10.1007/s10195-008-0038-y>
  4. L. Shi, Z. G. Guo, and W. M. Liu, The recent progress of tribological biomaterials. *Biosurface and Biotribology*, **1** (2015) 81. <https://doi.org/10.1016/j.bsbt.2015.06.002>
  5. C. Fabry, C. Zietz, R. Dammer, and R. Bader, 12 Patterns of Wear in Total Knee Replacement, *The Unhappy Total Knee Replacement*. (2015) 135-145 [https://doi.org/10.1007/978-3-319-08099-4\\_13](https://doi.org/10.1007/978-3-319-08099-4_13)
  6. S. Bahonar, Volumetric Wear Assessment and Characterization of Striated Pattern of Retrieved UHMWPE Tibial Insert Medicine, *Environmental Science*, 2015, Accessed: May 20, (2020) <https://pdfs.semanticscholar.org/cc0e/7ae4c4f6022ef1011014b4d9740e802fb8c3.pdf>
  7. G. W. Stachowiak, *Friction and Wear of Polymers*, Ceram-

- ics and Composites in Biomedical Applications, *Advances in Composite Tribology*. (1993) 509 <https://doi.org/10.1016/b978-0-444-89079-5.50018-0>
8. J. Baena, J. Wu, and Z. Peng, Performance of UHMWPE and Reinforced UHMWPE Composites in Arthroplasty Applications: A Review, *Lubricants*, **3** (2015) 413-436, <https://doi.org/10.3390/lubricants3020413>
  9. Lapaj and J. Rozwalka, Retrieval analysis of TiN (titanium nitride) coated knee replacements: Coating wear and degradation in vivo, *J. Biomed. Mater. Res. B Appl. Biomater.*, **108** (2020) 1251.
  10. S. Bahonar, Volumetric Wear Assessment and Characterization of Striated Pattern of Retrieved UHMWPE Tibial Inserts, *Medicine, Environmental Science*, 2015, Accessed: May 20, (2020). <https://pdfs.semanticscholar.org/cc0e/7ae4c4f6022ef1011014b4d9740e802fb8c3.pdf>
  11. P. Massin “How does total knee replacement technique influence polyethylene wear?”, *Orthop. Traumatol. Surg. Res.*, **103** (2017) S21.
  12. S. V. Panin, L. A. Kornienko, M. V. Chaikina, V. P. Sergeev, L. R. Ivanova, and S.V.Shiko. Nano- and micro-structured UHMWPE composites filled with hydroxyapatite irradiated by nitrogen ion beams for bio.medical applications, *Russ. Phys. J.* **56** (2014) 1137.
  13. B. Peng Chang, H. Md. Akil, R. Bt Nasir, and A. Khan. Optimization on wear performance of UHMWPE composites using response surface methodology, *Tribol Int*, **88** (2015) 252.
  14. A. Golchim, A. Wikner, and N. Emami, An investigation into tribological behavior of multi-walled carbon nanotube/graphene oxide reinforced UHMWPE in water lubricated contacts, *Tribol. Int.* **95** (2016) 156.
  15. Y. Xue, W. Wu, O. Jacobs, and B. Schädel, Tribological behavior of UHMWPE/HDPE blends reinforced with multi-wall carbon nanotubes, *Polym. Test* **25** (2006) 221.
  16. A. Fonseca, S. Kananraj, M. S. A. Oliveira, and J. A. O. Simpers, Enhanced UHMWPE Reinforced with MWCNT through Mechanical Ball-Milling, *Defect and Diffusion Forum*, **312** (2011) 1238, <https://doi.org/10.4028/www.scientific.net/ddf.312-315.1238>.
  17. N. Avinash Patil, J. Njuguna, and B. Kandasubramanian, UHMWPE for biomedical applications: Performance and functionalization, *Eur. Polym J*, **125** (2020) 109529.
  18. M.A.Samad and S.K. Sinha. Mechanical thermal and tribological characterization of a UHMWPE films reinforced with carbon nanotubes coated on steel, *Tribol Int*, **44** (2011) 1932,
  19. J. M. Diabb Zabala *et al.*, Manufacture and mechanical properties of knee implants using SWCNTs/UHMWPE composites, *J Merch Behav Matter*, **120** (2021) 104554.
  20. M. J. Martinez-Morlanes, P. Castell, V. Martinez-Nogues, M.T Martinez,, P. J. Alonso, and J. A Puertolas. Effects of gamma-irradiation on UHMWPE/MWNT nanocomposites, *Composites Science and Technology*, **71** (2011) 282, <https://doi.org/10.1016/j.compscitech.2010.11.013>.
  21. M. J. Martinez-Morlanes, P. Castell, P. J. Alonso, M. T. Martinez, and J. A. Puertolass, Multi-walled carbon nanotubes acting as free radical scavengers in gamma-irradiated ultra-high molecular weight polyethylene composites, *Carbon*, **50** (2012) 2442, <https://doi.org/10.1016/j.carbon.2012.01.066>.
  22. S. L. Ruan, P. Gao, X. G. Yang, and T.X. Yu, Toughening high performance ultrahigh molecular weight polyethylene using multiwalled carbon nanotubes, *Polymer*, **44** (2003) 5643,
  23. Y.-S. Zoo, J.-W. An, D.-P. Lim, and D.-S. Lim, Effect of Carbon Nanotube Addition on Tribological Behavior of UHMWPE, *Tribology Letters*, **16** (2004) 305, <https://doi.org/10.1023/b:tril.0000015206.21688.87>.
  24. S. Kanagaraj, M. T. Mathew, A. Fonseca, M. S. A. Oliveira, J. A. O. Simoes, and L. A. Rocha, Tribological characterisation of carbon nanotubes/ultrahigh molecular weight polyethylene composites: the effect of sliding distance, *International Journal of Surface Science and Engineering*, **4** (2010) 305 <https://doi.org/10.1504/ijsurfse.2010.035138>.
  25. N. Camacho, E. A. Franco-Urquiza, and S. W. Stafford, Wear performance of multiwalled carbon nanotube-reinforced ultra-high molecular weight polyethylene composite, *Advances in Polymer Technology*, **37** (2018) 2261, <https://doi.org/10.1002/adv.21885>.
  26. G. Del Prado *et al.*, DLC coatings for UHMWPE: Relationship between bacterial adherence and surface properties, *Journal of Biomedical Materials Research Part A*, **100A** (2813)
  27. S. H. Teoh, R. Thampuran, and W. K. H. Seah, Coefficient of friction under dry and lubricated conditions of a fracture and wear resistant P/M titanium-graphite composite for biomedical applications, *Wear*, **214** (1998) 237, [https://doi.org/10.1016/s0043-1648\(97\)00231-7](https://doi.org/10.1016/s0043-1648(97)00231-7).
  28. L. Yong, C. Wei, L. Yang, M. Tian, H. Xuo, and W. Chen, The surface characterization of microporous titanium carbide coating on titanium alloys, *Proceedings of the Institution of Mechanical Engineers, Part J: Journal of Engineering Tribology*, **228** (2014) 521. <https://doi.org/10.1177/1350650113517375>.
  29. Y. Luo, S. Ge, H. Liu, and Z. Jin, Microstructure analysis and wear behavior of titanium cermet femoral head with hard TiC layer, *Journal of Biomechanics*, **42** (2009) 2708. <https://doi.org/10.1016/j.jbiomech.2009.08.003>.
  30. C. V. R. Meenakshi, and S. V. Ramana, Nano Coatings on Knee Implants A Tribological Review, *Materials Today: Proceedings*, **22** (2020) 2088.
  31. S. Deenoi and S. Dechjarer, Effect of Cryogenic and Coating treatments on Wear and Friction between Titanium Alloy and UHMWPE for Knee Implants, *Materials Today: Proceedings*, **17** (2019) 1939.
  32. V. A. Gonzalez-Mora, M. Hoffmann, R. Stroosnijder, and F. Javier Gil, The role of hardness and roughness on the wear of different CoCrMo counterfaces on UHMWPE for artificial joints, *J. Biomed. Sci. Eng.* **4** (2011) 651.
  33. R. P. van Hove, I. N. Sierevelt, B. J. van Royen, and P. A. Nolte. Titanium-Nitride Coating of Orthopaedic Implants: A Review of the Literature, *Biomed Res. Int.*, **2015** (2015), <https://doi.org/10.1155/2015/485975>.

34. N. Camacho, S. Stafford, K. Garza, R. Suro, and K. Barron, Ultra-High Molecular Weight Polyethylene Reinforced with Multiwall Carbon Nanotubes: In Vitro Biocompatibility Study Using Macrophage-Like Cells, *Lubricants*, **3** (2015) 597, <https://doi.org/10.3390/lubricants3030597>.
35. F. Committee and F04 Committee, Test Method for Wear Testing of Polymeric Materials Used in Total Joint Prostheses. <https://doi.org/10.1520/f0732-00r11>.
36. J. P. Perdew, K. Burke, and M. Ernzerhof, Generalized Gradient Approximation Made Simple, *Phys. Rev. Lett.*, **77** (1996) 3865.
37. M. D. Segall *et al.*, First-principles simulation: ideas, illustrations and the CASTEP code, *J. Phys. Condens. Matter*, **14** (2002) 2717.
38. T. Y. Tan, J. Li, and S. Y. Gao, A first principles investigation on the mechanism of TiC act as heterogeneous nucleation substrate of Mg phase to refine grains in AZ91, *AIP Adv.*, **9** (2019) 085105.
39. A. Dorner-Reisel, C. Schürer, and E. Müller, The wear resistance of diamond-like carbon coated and uncoated Co28Cr6Mo knee prostheses, *Diam. Relat. Mater.*, **13** (2004) 823.
40. J. I. Oñate *et al.*, Wear reduction effect on ultra-high-molecular-weight polyethylene by application of hard coatings and ion implantation on cobalt chromium alloy, as measured in a knee wear simulation machine, *Surface and Coating Technology*, **142-144** (2001) 1056. [https://doi.org/10.1016/0257-8972\(01\)01074-x](https://doi.org/10.1016/0257-8972(01)01074-x).
41. M. Jelinek *et al.*, Dual laser deposition of Ti:DLC composite for implants, *Laser Physics*, **26** (2016) 105605. <https://doi.org/10.1088/1054-660x/26/10/105605>.
42. J. Cui, L. Qiang, B. Zhang, X. Ling, T. Yang, and J. Zhang, Mechanical and tribological properties of Ti-DLC films with different Ti content by magnetron sputtering technique, *Applied Surface Science*, **258** (2012) 5025. <https://doi.org/10.1016/j.apsusc.2012.01.072>.
43. Q. Wang *et al.*, Influence of Ti content on the structure and tribological properties of Ti-DLC coatings in water lubrication, *Diamond and Related Materials*, **25** (2012) 163. <https://doi.org/10.1016/j.diamond.2012.03.005>.
44. M. Viljus, J. Pirso, K. Juhani, and S. Letunovits, Structure Formation in Ti-C-Ni-Mo Composites during Reactive Sintering, *Materials Science*, **18** (2012) 1343, <https://doi.org/10.5755/j01.ms.18.1.1343>.
45. S. Affatato, E. Modena, S. Carmignato, and P. Taddei, The use of Raman spectroscopy in the analysis of UHMWPE unicondylar bearing systems after run on a force and displacement control knee simulators, *Wear*, **297** (2013) 781.
46. G. R. Strobl and W. Hagedorn, Raman spectroscopic method for determining the crystallinity of polyethylene, *Journal of Polymer Science: Polymer Physics Edition*, **16** (1978) 1181.
47. S. Osswald, M. Havel, and Y. Gogotsi, Monitoring oxidation of multiwalled carbon nanotubes by Raman spectroscopy, *J. Raman Spectrosc.*, **38** (2007) 728.
48. A. C. Ferrari, Raman spectroscopy of amorphous, nanostructured, diamond-like carbon, and nanodiamond, *Philosophical Transactions of the Royal Society A*, **362** (2004) 1452, <https://doi.org/10.1098/rsta.2004.1452>.
49. Z. Liu and T. H. C. Childs, The influence of TiC, CaF2 and MnS additives on friction and lubrication of sintered high speed steels at elevated temperature, *Wear*, **193** (1996) 31, [https://doi.org/10.1016/0043-1648\(95\)06652-7](https://doi.org/10.1016/0043-1648(95)06652-7).
50. M. Yang, C. Zheng, J. Ran, W. Zhang, and Z. Li, Studies on properties of biofriction and wear for friction pairs of UHMWPE and Ti matrix-TiN-TiC gradient film materials], *Sheng Wu Yi Xue Gong Cheng Xue Za Zhi*, **17** (2000) 1.
51. The structural and mechanical characterization of TiC and TiC/Ti thin films grown by DC magnetron sputtering, *J. Eur. Ceram. Soc.*, **38** (2018) 2886.
52. M. Nine, D. Choudhury, A. Hee, R. Mootanah, and N. Osman, Wear Debris Characterization and Corresponding Biological Response: Artificial Hip and Knee Joints, *Materials*, **7** (2014) 980. <https://doi.org/10.3390/ma7020980>.
53. L. Wang, T. Fang, and J.H. Gong. First-Principles Study of TiC(111) Surface, *Appl. Mech. Mater.*, **229-231** (2012) 82.